Journal of Materials Chemistry A

Accepted Manuscript

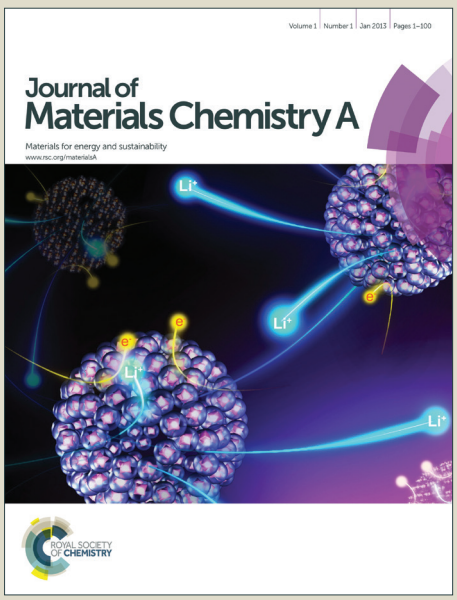

ROYAL SOCIETY OF CHEMISTRY

www.rsc.org/materialsA

Hierarchical core/shell meso-ZSM-5@mesoporous aluminosilicate-supported Pt nanoparticles for bifunctional hydrocracking

Darui Wang, Le Xu, Peng Wu*

Shanghai Key Laboratory of Green Chemistry and Chemical Processes, Department of Chemistry, East China Normal University, North Zhongshan Rd. 3663, Shanghai 200062, P. R. China

E-mail: pwu@chem.ecnu.edu.cn

Tel/Fax: 86-21-62232292

Abstract

A series of well-defined core/shell-structured composite materials comprising microporous/mesoporous ZSM-5 as core and mesoporous alumionosilicate as shell were synthesized by combining controlled desilication with sodium hydroxide solution and subsequent self-assembly with triblock copolymer. An aluminosilicate shell with uniform mesopores was grown closely around the crystals of mesoporous ZSM-5, with a tunable thickness of 60 - 300 nm by adjusting the extent of desilication. The obtained composite zeolites exhibited a hierarchical porosity containing original regular MFI micropores (ca. 0.56 nm) and desilication-induced randomly distributed mesopores (5 - 50 nm) both within core ZSM-5 crystals as well as relatively uniform mesopores (ca. 6 nm) inside the shell part on zeolite surface. The mesoporous aluminosilicate shell, self-assembled from the MFI zeolite fragments as a result of partially dissolved ZSM-5 crystals, demonstrated weak acidity and much higher hydrothermal stability in comparison to the shell synthesized by additional silica source. Taking advantage of the confining effect of the mesopores, Pt nanoparticles were incorporated into the mesoporous shells, giving rise to bifunctional catalysts which exhibited a higher selectivity of C_5 - C_{11} liquid products than conventional Pt/ZSM-5 catalyst in the hydrocracking of *n*-hexadecane.

Keywords:

ZSM-5

Desilication

Core-shell

Hierarchical zeolites

n-Hexadecane

Hydrocracking

1 Introduction

Hydrocracking of heavy oil for the production of high-value middle distillates, e.g., gasoline, diesel and jet fuel, plays an important role in petroleum industries.[1-5] Present hydrocracking process are faced with major challenges, for instance, heavy oil contains bulky molecules which have difficult mass transportation to the active sites located inside the zeolite micropores.[6,7] Integrating mesopores into microporous zeolites would circumvent the diffusion limitation imposed by the small pore sizes of zeolites and make them applicable for catalysis containing bulky molecules. Moreover, it also provides opportunities to synthesize bifunctional catalysts with different active sites spatially separated in micropores and mesopores. In recent years, extensive research efforts have been devoted to synthesize hierarchical porous composite zeolites with the purpose to reduce the diffusion limitation and to take advantage of the microporosity in processing bulky reactants, including post-desilication and dealumination,[8-17] chemical treatment,[18] as porogen-assisted synthesis.[19-28] These materials provide opportunities to prepare mesoporosity-derived multifunctional catalysts with differently distributed active sites in zeolites. The post-syntheses introduce mesoporosity effectively into zeolite crystals, but also exhibit the advantages of less cost in comparison to the direct synthesis requiring expensive organic additives. Steaming dealumination is widely employed to create mesopores within FAU and MOR zeolites.[29,30] In addition, alkaline-assisted desilication proves to be a more effective and versatile approach for introducing mesopores into a variety of zeolites, such as MFI,[31] BEA,[32] FER,[33] MWW,[34] MOR[35] and AST.[36] The formed

mesopores penetrate randomly throughout the crystals in a disordered manner. It is, therefore, highly desirable to develop a more controllable methodology for constructing hierarchical pore structure inside zeolites.

Recently, great efforts have been devoted to the design and controlled fabrication of hierarchical materials with novel structures, such as core-shell,[37,38] hollow sphere[39] and rattle-type[40] materials. Among them, the core-shell hybrid materials consisting of zeolite crystal cores and mesoporous silica shells form a class of promising catalysts applicable to dsorption and separation,[41,42] drug delivery,[43,44] catalysis etc.[37,38,45-47] In particular, combining zeolites and mesosilica together, the bimodal core-shell materials provide new opportunities for preparing bifunctional or multifunctional catalysts with spatially separated active sites.

To design such core-shell materials containing a mesoporous shell, the most important step is to introduce an oriented mesophase shell onto the core surface. Yu et al. once prepared uniform core-shell materials silicalite-1@mesosilica using relatively expensive octadecyltrimethoxysilane as mesopore directing agent and additional silica source of tetraethoxysilane (TEOS).[48] Similarly, Han et al. synthesized the core-shell structured zeolite@mesosilica using less expensive cetyltrimethylammonium bromide (CTAB) as a template but without addition of silica source,[49] in which the mesosilica shell was self-assembled from the silica species leached from the zeolite crystals in an ammonia solution, and the shell thicknesses were tuned conveniently by prolonging the hydrothermal treatment to dissolve more silica species. Recently, we prepared core-shell structured TS-1@mesosilica and further incorporated the Au nanoparticles

into mesosilica shell, resulting in a bifunctional catalyst useful to direct gas-phase epoxidation of propylene to propylene oxide with H_2 and O_2. The Au NPs served as the catalytic active sites for *in situ* formation of H_2O_2 from H_2 and O_2, while the tetrahedral Ti species were useful for the selective epoxidation of alkenes with H_2O_2.[37] Moreover, we have succeeded in synthesizing a center radially fibrous silica encapsulated TS-1 (TS-1@KCC-1) in a microemulsion system for the first time. Supporting $Rh(OH)_3$ species on this composite material gave rise to a robust bifunctional catalyst for one-pot synthesis of benzamide from benzaldehyde, ammonia and hydrogen peroxide. The TS-1 core catalyzed the oxidation of ammonia by hydrogen peroxide to synthesize hydroxylamine intermediate; this intermediate then reacted with an aldehyde via non-catalytic oximation to produce an aldoxime. The aldoxime was then transformed into primary amide, catalyzed by the $Rh(OH)_3$ species on TS-1@KCC-1.[50] Aforementioned literature survey indicates that the cationic surfactant CTAB is prior to orient a mesosilica shell aligned on silica-based cores in basic media. However, the size of resultant mesopores is usually below 5 nm. It is preferable to use a bulky polymer surfactant as template with the aim of preparing mesosilica with larger ordered pores (>5 nm) to extend application variety. Through adjusting the pH value of synthetic solution to well-matched isoelectric points between TS-1 crystal and silica gel, we synthesized a bimodal porous material by coating TS-1 with mesosilica shell directly templated by triblock copolymer P123.[51] On the other hand, Qian et al. developed a facile coating strategy in a ultra-dilute acidic medium using triblock copolymer as a template for the preparation of core-

shell structured composite ZSM-5@SBA-15, which showed an excellent catalytic performance in methanol-to-propylene conversion.[38] However, the core-shell structured composite of microporous/mesoporous zeolite as core and mesoporous aluminosilicate as shell has not been reported yet, especially without any additional silica source. To the best of our knowledge, a similar core-shell structured composite has only been reported by Han et al.,[49] in which the ammina/CTAB system was employed, forming a limited amount of mesopores inside zeolite core. Therefore, it is also a big challenge to design novel core-shell structured materials in order to enhance the accessibility of microporous core where the catalytically active sites exist.

We report here the synthesis of the core-shell structured composites composed of ordered mesoporous aluminosilicate shell and mesopore-containing ZSM-5 core. This material possessed the hierarchical pores interconnecting with each other, and a gradient acidity distribution from shell to core, and a great hydrothermal stability as well. Further incorporating Pt nanoparticles into mesoporous shell led to bifunctional catalysts efficient for the hydrocracking of *n*-hexadecane.

2 Experimental section

2.1 Synthesis of ZSM-5 zeolite

ZSM-5 zeolites were synthesized with the assistant of active seeds. The active seeding gel was prepared by the following procedure. Tetraethyl orthosilicate (TEOS) was dropped into the solution containing water and tetrapropylammonium hydroxide (TPAOH, 25 % aqueous solution). After homogenizing at 353 K for 2 h, the synthetic gel with a molar composition of 1.0 TEOS : 0.15 TPAOH : 14 H_2O was introduced

into a Teflon-lined steel autoclave and aged at 393 K for 3 h. After cooling, the obtained seeding gel was directly used for the synthesis of ZSM-5 zeolites without any treatment.

ZSM-5 zeolite was synthesized from piperidine (PI) as structure directing agent (SDA), silica sol (30 wt.% SiO_2), aluminum sulfate and sodium hydroxide. Sodium hydroxide and aluminum sulfate were first dissolved in the aqueous solution of piperidine. Silica sol and active seeding gel were then dropped into the above solution and further stirred for 30 minutes, forming a gel composition of 1.0 TEOS : 0.0125 Al_2O_3 : 0.2 PI : 0.05 Na_2O : 25 H_2O. SiO_2 in the active seeding gel accounted for 1 % of the whole SiO_2 in gel. The gel was crystallized in a Teflon-lined steel autoclave at 443 K for 72 h. The ZSM-5 product was collected by filtration, dried at 373 K overnight, and then calcined in air at 823 K for 6 h to remove the organic species occluded. The resulting ZSM-5 was brought into ammonium form via three consecutive exchanges in 1 M ammonium chloride solution at 353 K for 2 h. After filtration, washing and drying overnight at 373 K, the ammonium ion-exchanged zeolite was subsequently calcined at 823 K for 6 h to give proton-type ZSM-5.

2.2 Preparation of MZ@MSA core-shell composite materials

The core/shell-structured composite MZ@MSA, comprising mesoporous ZSM-5 core and mesoporous aluminosilicate shell, was synthesized in two separated processes, that is, controlled desilication and self-assembly using triblock copolymer P123 (polyethylene-polypropylene glycol) as template without additional silica source. In a typical synthesis of MZ@MSA with a shell thickness of approximate 150 nm, 1 g

of ZSM-5 nanocrystals (1 g, Si/Al=38) was desilicated in 50 mL of 0.2 M NaOH solution containing piperidine (PI/SiO_2 molar ratio of 0.02) at 338 K for 30 min. Piperidine added was expected to serve as protecting agent to avoid a deep destroying of the fundamental building units of ZSM-5, the piperidine may enter into the zeolite pores and effectively limited the silicon hydrolysis and derived mesopore formation. During desilication, the ZSM-5 crystals were partially dissolved, leading to mesoporous ZSM-5 and leached silica or alumina fragments in solution. Next, deionized water (130 mL) and 76.0 g of absolutely ethanol containing P123 (2.0 g) were added into the above mixture. Then, a desirable amount of HCl solution (0.5 M) was added dropwise into the mixture to adjust pH to ca. 5.2 under continuous stirring to well-matched isoelectric points between mesoporous ZSM-5 and silica gel, which was stirred for 30 min and ultrasonicated for another 30 min to form a uniform suspension. After reaction at 308 K for 48 h, the reaction mixture was further heated at 343 K for 24 h. Through this step of self-assembly, leached silica or alumina species were reassembled on the surface of mesoporous ZSM-5 to form core-shell structured materials. The white solid precipitate was separated by filtration, washed with deionized water and ethanol in turn for three times, and dried at 353 K overnight. The samples were calcined to remove organic species at 823 K for 6 h. The shell thickness was tuned by changing the concentration of alkaline solution or by addition of piperidine during desilication. The samples were denoted as MZ_x@MSA, where *x* represents the desilicated condition. In the case of $MZ_{AT0.2\text{-}PI0.02}$@MSA, 0.2 indicates the molar concentration of NaOH, while 0.02 represents the PI/SiO_2 molar ratio. For

control experiment, the sample of $MZ_{AT0.2\text{-}PI0.02}$ was prepared by desilication only, while Al-containing mesoporous silica, denoted as MSA, was prepared by following the same procedures mentioned above but using only the filtrate obtained by decompress filtration as silica and aluminum sources after removing undissolved bulky ZSM-5 particles.

2.3 Preparation of Pt/MZ@MSA and Pt/ZSM-5 materials

The precise metal active components were introduced into the core/shell samples by the impregnation techniques described previously,[52] using $H_2PtCl_6 \cdot 6H_2O$ as precurosr to obtain a content of about 1 wt.% Pt. The metal solution was added to the samples at room temperature and stirred for 20 h to reach adsorption equilibrium. Then, the remaining solution was removed by evaporation. The sample was dried at 353 K for 6 h, followed by calcination under a N_2 flow (12 L h^{-1} g^{-1}) at 673 K for 2 h to allow the decomposition of the Pt precursor and reduction in a H_2 flow (12 L h^{-1} g^{-1}) at 673 K for 3 h. Pt/ZSM-5 catalyst was prepared using the same procedures for comparison.

2.4 Characterization methods

Powder X-ray diffraction (XRD) was employed to check the structure and crystallinity of the zeolites. The XRD patterns were collected on a Rigaku Ultima IV diffractometer using Cu Kα radiation at 30 kV and 25 mA. Nitrogen gas adsorption measurements were carried out at 77 K on a BEL-MAX gas/vapor adsorption instrument. The samples were evacuated at 573 K for at least 6 h before adsorption. The *t*-plot method was used to discriminate between micro- and mesoporosity. The

mesopore size distribution was obtained by the BJH model from the adsorption branch of the isotherms. Si and Al contents were determined by inductively coupled plasma emission spectrometry (ICP) on a Thermo IRIS Intrepid Ⅱ XSP atomic emission spectrometer. The IR spectra were collected on Nicolet Nexus 670 FT-IR spectrometer in absorbance mode at a spectral resolution of 4 cm^{-1}. The sample was pressed into a self-supported wafer with 4.8 mg cm^{-2} thickness, which was set in a quartz cell sealed with CaF_2 windows and connected to a vacuum system. After evacuated at 723 K for 2 h, adsorption was carried out by exposing the pretreated wafer to a pyridine vapor at 298 K for 0.5 h. The adsorbed pyridine was evacuated successively at 423 K for 1 h. The spectra were collected at room temperature. Acidity was measured by temperature-programmed desorption of ammonia (NH_3-TPD) with a Micrometrics tp-5080 equipment equipped with a thermal conductivity detector (TCD) detector. Typically, 100 mg of sample was pretreated in helium stream (30 mL/min) at 823 K for 1 h. The adsorption of NH_3 was carried out at 323 K for 1 h. The catalyst was flushed with helium at 373 K for 2 h to remove physisorbed NH_3 from the catalyst surface. The TPD profile was recorded at a heating rate of 10 K/min from 373 K to 873 K. Scanning electron microscopy (SEM) was performed on a Hitachi S-4800 microscope to determine the morphology. Transmission electron microscopy (TEM) images were collected on a Tecnai G^2 F30 microscope after the samples were deposited onto a holey carbon foil supported on a copper grid.

2.5 Hydrocracking of *n*-hexadecane

The catalytic performance of core-shell composites in the hydrocracking of *n*-hexadecane was evaluated in a continuous fixed-bed quartz reactor (i.d. 25 mm). The catalyst (0.2 g) centered at the reactor was activated in a furnace at 703 K for 1 h in H_2 atmosphere in the reactor before the reaction, and then the reactor was cooled to the reaction temperatures (533 - 653 K). Afterwards, a co-feed of H_2 and *n*-hexadecane was introduced at a H_2/C_{16} molar ratio of 35. The weight hourly space velocity (WHSV) of *n*-hexadecane was varied in the range of 1 - 16.2 h^{-1} by changing the flow rate of C_{16} from 0.1 to 1.62 g h^{-1}. The reaction products were analyzed by an on-line gas chromatograph equipped with an FID detector and a GsBP-1 capillary column (50 m×0.53 mm×3.0 μm).

3 Results and discussion

3.1 Preparation and characterizations of MZ_x@MSA materials

Powder X-ray diffraction (XRD) investigations permit the characterization of the order of micro- and mesoporous materials by analyzing their pore packing. Fig. 1 shows the XRD patterns of core–shell $MZ_{AT0.2\text{-}PI0.02}$@MSA and related precursor materials. $MZ_{AT0.2\text{-}PI0.02}$ was characteristic of crystalline zeolites in the 2θ region of 5 - 35°, which corresponded to a typical structure with the MFI topology (Fig. 1b). As the crystalline part was partially desilicated, its intensity was reasonably weaker than that of pure ZSM-5 crystal (Fig. 1a). Unlike $MZ_{AT0.2\text{-}PI0.02}$, a new diffraction due to the mesophase was observed for $MZ_{AT0.2\text{-}PI0.02}$@MSA around 2θ = 1.0º in the lower angle region (Fig. 1d), which is attributed to the mesostructure in the shell part formed by self-assembly.[53] The reflection peak at around 1.0º was relatively broad and poorly

resolved, implying a disordered array of the mesopores different from a hexagonal symmetry. The weakening of the MFI structure-related diffractions for $MZ_{AT0.2\text{-}PI0.02}$@MSA was simply because of a diluting effect of mesophase shell on the crystalline component ZSM-5 in the composite. The intensity of the reflection at 1.0º changed with varying the conditions of alkaline treatment. This reflection slightly increased with increasing the concentration of alkaline solution from 0.1 M NaOH (Fig. 1c) to 0.2 M NaOH in the presence of piperidine (Fig. 1d), as the proportion of mesophase to ZSM-5 became higher. However, when the pretreatment was carried out first in 0.2 M NaOH but in the absence of piperidine and then the assembly of mesophase shell was conducted, the reflection at 1.0º became broader and slightly decreased in intensity (Fig. 1e), in comparison to the case of 0.2 M NaOH treatment in the presence of piperidine. As more silica/alumina species would be leached out of ZSM-5 crystals without the protection of piperidine, the mesophase became more disordered in pore array, and the diffractions in high angle region, contributed by ZSM-5 crystals, decreased with increasing the concentration of alkaline solution.

The SEM and TEM images were taken to investigate the morphology and mesostructure of MZ_x@MSA. The pristine ZSM-5 crystals exhibited a cross-shaped morphology with an average particle size of around 2 μm (Fig. 2a and 2b). When ZSM-5 was subjected to the alkaline treatment with NaOH in the presence of piperidine, the crystals were etched to give a rougher surface due to silica leaching (Fig. 2c). Obviously, the mesopores were introduced into the crystals of $MZ_{AT0.2\text{-}PI0.02}$, which can be inferred from the black doped with white dots in TEM image (Fig. 2d).

The core-shell structured materials templated by P123 had an obviously enlarged particle size in comparison to $MZ_{AT0.2\text{-}PI0.02}$ and a new phase was visible even under SEM microscope grown around the $MZ_{AT0.2\text{-}PI0.02}$ crystals (Fig. 2e). In agreement with the SEM images, the TEM images showed that the shell thickness increased from 60 nm up to 300 nm by simply intensifying the alkaline treatment conditions (Fig. 2f and 2g). Although SBA-15 mesoporous silica with a highly ordered hexagonal structure was obtained in the absence of ZSM-5 particles, the channel array within the mesoporous silica shell of the present MZ_x@MSA obviously lacked the hexagonal symmetry but was of a disordered manner. It is understandable that there is difficulty in coating a two-dimensional structure with a hexagonal symmetry on the irregular surface of the 3D spheres. In contrast, the wormhole-like pore structure may make the mesopores in shell have more chances to interconnect the micropores inside meso-ZSM-5 core in comparison to ordered hexagonal channels. This kind of pore structure has the advantage of taking full use of the whole porosities, which is important to make the acid sites in meso-ZSM-5 accessible from outside in terms of catalytic applications.[51] Mesosilica is very sensitive to electron irradiation at the very high magnification in TEM measurements, but high-resolution TEM (HRTEM) imaging still provided reliable information confirming the formation of the core–shell structure. The HRTEM images revealed that there was a close connection between the mesosilica shell and meso-ZSM-5 core. A representative HRTEM image showed the junction between the shell and core (Fig. 3A and Fig. S1 in supplemental materials), in which the MFI crystalline phase and the mesoporous silica shells grew connectedly.

The HRTEM image taken at the core-shell cross section demonstrated three kinds of pores from opened mesoporous shell to accessible micro/mesoporous core: uniform mesopores on the surface of the zeolite crystals templated by P123 (Fig. 3Ba), original 10-memrbed ring (MR) micropores of ZSM-5 (Fig. 3Bb) and irregular intracrystal mesopores created by desilication (Fig. 3Bc). A rapid damage of the mesopore shell under electron-beam irradiation in the high-resolution mode of TEM investigation resulted in difficulties in simultaneously capturing clear pore images of mesosilica shell and meso-ZSM-5 core.[54]

The pristine ZSM-5 sample showed a type I adsorption isotherm, in which the adsorption amount was saturated in an extremely low relative pressure region ($P/P_0 <$ 0.05) as a result of monolayer adsorption of N_2 inside the micropores (Fig. 4Aa). $MZ_{AT0.2\text{-}PI0.02}$ was characteristic of a type combined type I ($P/P_0 < 0.05$) and type IV (in the P/P_0 range of 0.7 - 1.0) (Fig. 4Ab), which indicated the formation of a hierarchical porous system containing both micropores and mesopores. However, the $MZ_{AT0.2\text{-}PI0.02}$@MSA sample showed a sharp uptake at a relative pressure ($P/P_0 < 0.05$) (type I), type IV curves with a capillary condensation at P/P_0 of 0.5 - 0.8 and a similarity to H2 hysteresis loop in desorption isotherm, as well as a third step in higher relative pressure region of ($P/P_0 =$ 0.7 - 1.0). The third adsorption step was the same as that in $MZ_{AT0.2\text{-}PI0.02}$, corresponding to the adsorption in the mesopores introduced into ZSM-5 core by desilication or the adsorption/condensation on particle surface. In contrast to the parent ZSM-5 sample with only 10-MR micropores of ca. 0.56 nm, the $MZ_{AT0.2\text{-}PI0.02}$ sample showed a bimodal pore size distribution (Fig. 4B),

that is, micorpores located at ca. 0.56 nm and mesopores of 5 - 50 nm attributed to the irregular mesopores introduced into ZSM-5 by desilication. Moreover, the $MZ_{AT0.2\text{-}PI0.02}$@MSA sample showed three levels of pore size distribution, that is, uniform mesopores of 6.2 nm P123-assembled on zeolite crystal surface and the same bimodal pores as $MZ_{AT0.2\text{-}PI0.02}$.

The special surface area obtained by the BET method from the adsorption branch (S_{BET}), the total pore volume (V_{tot}) and the external surface area (S_{ext}) of pristine ZSM-5 were 316 $m^2\ g^{-1}$, 0.21 $cm^3\ g^{-1}$, and 12 $m^2\ g^{-1}$, respectively (Table 1, No. 1). After desilication by NaOH with additional piperidine, the S_{BET}, V_{tot} and S_{ext} increased to 452 $m^2\ g^{-1}$, 0.72 $cm^3\ g^{-1}$, and 220 $m^2\ g^{-1}$, respectively (Table 1, No. 2). After coated with a mesoporous silica shell on the meso-ZSM-5 core, the S_{BET} and S_{ext} further increased to 539 $m^2\ g^{-1}$ and 358 $m^2\ g^{-1}$, respectively, but V_{tot} decreased from 0.72 $cm^3\ g^{-1}$ to 0.61 $cm^3\ g^{-1}$, (Table 1, No. 4), probably due to a part of intracrystal mesopores (5 - 50 nm) introduced by desilication were replaced by smaller mesopores (6.2 nm) formed by P123 templating. Also it was reflected in the pore size distribution (Fig. 4B), the peak located from 5 nm to 50 nm for $MZ_{AT0.2\text{-}PI0.02}$@MSA was visibly lower than that for $MZ_{AT0.2\text{-}PI0.02}$. The reduction of micropore surface areas and volumes should be largely attributed to the reduced portion of ZSM-5 as a result of silica leaching and mesopore shell formation. The porosity of meso-/micropores for the core-shell structured composite materials can be tuned with a change of shell thickness from 60 to 300 nm by adjusting the NaOH concentration from 0.1 M to 0.2 M (Table 1, Nos. 3 - 5).

Apart from the disordered mesopores penetrating randomly throughout the crystals, the yield of desilicated materials was relatively low, which was defined as grams of solid after workup per gram of used ZSM-5. The yield of alkaline-treated sample $MZ_{AT0.2}$ without piperidine was only 43% (Table 1, No. 5 and Fig. S2), the yield of $MZ_{AT0.2\text{-}PI0.02}$ increased to 69 % (Table 1, No. 4 and Fig. S2) when desilicated with 0.2 M NaOH with additional piperidine as a protective agent. In the case of the treatment with 0.1 M NaOH, the yield was further increased to 81 % (Table 1, No. 3 and Fig. S2) for $MZ_{AT0.1}$, indicating 20 % silica (possibly containing also a small amount of Al species also) was leached from ZSM-5 crystals under a lower NaOH concentration. In addition, with increasing the concentration of alkaline solution, more partially dissolved nanocrystals would fall off from the bulky aggregates of ZSM-5, then the absolute amount of aluminum species contained in the mesoporous shell would increase. Fortunately, when the core-shell structured composite materials were synthesized in two separated processes, that is, desilication first and subsequent self-assembly with P123 copolymer, the yields of MZ_x@MSA were maintained over 90 % (Table 1, Nos. 3 - 5, Fig. S2), indicating nearly most of the leached silica species were reassembled by P123 template, forming the shells of core-shell structured composite materials. This is of special importance in terms of applying the core-shell composite materials to industrial processes.

The self-assembled mesoporous shell from the aluminosilicate species leached out of ZSM-5 by desilication demonstrated an outstanding hydrothermal stability when compared with that using external tetraethylorthosilicate (TEOS) as silica

precursor. For comparison, a control sample $MZ_{AT0.2\text{-}PI0.02}$@MSA-TEOS was synthesized by self-assembling additional TEOS with P123 onto the $MZ_{AT0.2\text{-}PI0.02}$ sample after removing any silica/alumina species dissolved in filtrate. The shell thickness of the resultant sample MZAT0.2-PI0.02@MSA-TEOS was controlled to be the same as $MZ_{AT0.2\text{-}PI0.02}$@MSA by adjusting the ratio of TEOS/zeolite. The hydrothermal stability was investigated by treating $MZ_{AT0.2\text{-}PI0.02}$@MSA-TEOS and $MZ_{AT0.2\text{-}PI0.02}$@MSA in an autoclave at 403 K for 10 h, while the stability against steaming was checked by treating the same samples at 1023 K for 36 h in a flow of nitrogen saturated with water vapor at 373 K. The pristine samples of $MZ_{AT0.2\text{-}PI0.02}$@MSA-TEOS and $MZ_{AT0.2\text{-}PI0.02}$@MSA both showed a morphology without surface defects before hydrothermal treatment (Fig. 5a and 5b). After hydrothermal treatment at 403 K for 10 h, the mesoporous shell of $MZ_{AT0.2\text{-}PI0.02}$@MSA-TEOS was badly destroyed and peeled off seriously the zeolite core (Fig. 5d). In contrast, $MZ_{AT0.2\text{-}PI0.02}$@MSA well maintained the integral core-shell structure with only very few mesoporous shells were destroyed (indicated with the circle in Fig. 5c). Similarly, after experiencing a steaming treatment at 1023 K for 36 h, a great majority of mesoporous shells of $MZ_{AT0.2\text{-}PI0.02}$@MSA-TEOS flaked off and meso-ZSM-5 core exposed outside (Fig. 5f). In contrast, the morphology of $MZ_{AT0.2\text{-}PI0.02}$@MSA kept almost intact with only a small amount of mesoporous shell was destroyed by hydrolysis (Fig. 5e). The high hydrothermal stability of $MZ_{AT0.2\text{-}PI0.02}$@MSA should be closely related to the shell component. The component containing the MFI aluminosilicate species leached from as-synthesized ZSM-5 by alkaline treatment are

summed to resist a severe hydrothermal treatment. The novel shells of $MZ_{AT0.2\text{-}PI0.02}$@MSA had a "concrete with crushed stone"-like mesostructure, in which the MFI aluminosilicate species served as the "crushed stone", whereas the silica and alumina species of atomic level constituted a wormhole-like framework as the "cement".

To take a deep investigation into this issue, a pure Al-containing mesoporous silica (MSA) was skillfully synthesized by using the filtrate of $MZ_{AT0.2\text{-}PI0.02}$ as silica and alumina sources following the same synthesis procedure of core-shell composite. Although undissolved ZSM-5 solid was excluded, the XRD pattern of MSA still showed the characteristic diffractions due to the MFI topology at 2θ of 7.8º, 8.8º, 23.2º, 23.8º and 24.3º although weak in intensity (Fig. S3A). Meanwhile, the FT-IR spectrum of MSA showed the weak vibration band at 550 cm^{-1} and a strong one at 450 cm^{-1} (Fig. S3B), which are assigned to the asymmetric stretching mode of five-ring in the MFI framework and the Si-O bending mode, respectively.[55] XRD and FT-IR characterizations verified the existence of MFI structured component in MSA. As $MZ_{AT0.2\text{-}PI0.02}$@MSA was self-assembled taking the same procedures in the presence of alkaline-treated ZSM-5 crystals, its MSA shell would contain the MFI aluminosilicate species which served as the "crushed stone" and preserved a stable structure during hydrothermal treatment.

The ^{27}Al MAS NMR spectrum of pristine ZSM-5 showed only one signal of tetrahedral Al at 58 ppm but no resonance at 0 ppm due to octahedral Al (Fig. S4a), which meant that the Al ions were incorporated dominantly in the framework position.

The spectrum of $MZ_{AT0.2\text{-}PI0.02}$, obtained by desilication of ZSM-5, showed a broadened tetrahedral Al signal and the appearance of octahedral Al-relating signal (Fig. S4b). This implied that the dealumination of tetrahedral Al to the extraframework species took place partially along with the desilication by alkaline treatment, and the microenvironment of Al became more asymmetric in coordination states. However, the core-shell structured material of $MZ_{AT0.2\text{-}PI0.02}$@MSA showed only one signal of tetrahedral Al at 58 ppm as pristine ZSM-5, indicating that those octahedral Al species were converted back to tetrahedral ones during self-assembly process. It is assumed that the Al species would not be reinserted into the ZSM-5 framework but incorporated into the mesoporous SiO_2 part.

To explore the acidic properties systematically, five samples were taken into account, pristine ZSM-5 (Si/Al=38), desilicated sample of $MZ_{AT0.2\text{-}PI0.02}$ (Si/Al=28), a core-shell structured composite materials comprising of $MZ_{AT0.2\text{-}PI0.02}$ (Si/Al=28) core and Al-containing mesoporous shell with a thickness of 150 nm (denoted $MZ_{AT0.2\text{-}PI0.02}$@MSA), the mechanical mixture $MZ_{AT0.2\text{-}PI0.02}$&MSA containing contents of $MZ_{AT0.2\text{-}PI0.02}$ (76 wt.%) and MSA (24 wt.%), as well as pure Al-containing mesoporous silica. NH_3-TPD profiles of ZSM-5, $MZ_{AT0.2\text{-}PI0.02}$ and $MZ_{AT0.2\text{-}PI0.02}$&MSA mixture showed two clear peaks at 485 K and 677 K that corresponded to the weak and strong acid sites, respectively (Fig. 6a, 6b and 6d). Two desorption peaks at 480 K and 670 K were observed in the NH_3-TPD profile of $MZ_{AT0.2\text{-}PI0.02}$@MSA (Fig. 6c), which showed left-shifts relative to above three samples, which was in agreement with the results reported by Qian et al.[54] The pure Al-containing

mesoporous silica showed an extremely weak ammonia desorption peak at 473 K (Fig. 6e), corresponding to the weak acid sites. As shown in Table S1 in supplementary materials, the total acid quantity of $MZ_{AT0.2\text{-}PI0.02}$ was approximately 0.50 mmol g^{-1}, which was 0.03 mmolg^{-1} higher than that of pristine ZSM-5 (0.47 mmol g^{-1}) due to the decrease of Si/Al molar ratio from 38 to 28. The total acid quantity of $MZ_{AT0.2\text{-}PI0.02}$@MSA was approximately 0.35 mmol g^{-1}, corresponding to about 70.0 % that of $MZ_{AT0.2\text{-}PI0.02}$ and 74.5 % that of ZSM-5, respectively. $MZ_{AT0.2\text{-}PI0.02}$@MSA and $MZ_{AT0.2\text{-}PI0.02}$&MSA had very comparable acid amounts (0.35 vs 0.36 mmol g^{-1}), which was in agreement with the results reported previously.[38] The acid quantity of pure mesoporous material MSA was only 0.06 mmol g^{-1}, suggesting the main acid sites remained in the core part of ZSM-5 crystals. Pyridine-adsorption FT-IR spectra also clarified the change of the acidic properties (Fig. 7), the bands at around 1447 cm^{-1}, 1546 cm^{-1} and 1490 cm^{-1} are assigned to pyridine interacting with Lewis acid sites, Brønsted acid sites and both types of acid sites, respectively.[56] The band intensity at 1546 cm^{-1} for ZSM-5, $MZ_{AT0.2\text{-}PI0.02}$, $MZ_{AT0.2\text{-}PI0.02}$@MSA and $MZ_{AT0.2\text{-}PI0.02}$&MSA was much stronger than that of pure mesoporous MSA, which indicated that Brønsted acid sites dominated the total acid sites in zeolite-containing materials. However, MSA exhibited a much stronger band at 1447 cm^{-1} than the other samples, indicating the former contained mainly the Lewis acid sites. Thus, it is deduced that the shell part of $MZ_{AT0.2\text{-}PI0.02}$@MSA contributed to the Lewis acidity, while the mesoporous ZSM-5 core mainly gave the Brønsted acidity. A gradient acidity distribution would exist from the external shell to internal core in $MZ_{AT0.2\text{-}}$

$_{PI0.02}$@MSA.

In order to convert the core-shell composite materials into bifunctional catalysts, we supported Pt NPs on $MZ_{AT0.2\text{-}PI0.02}$@MSA using the impregnation method described by Coloma et al.[52] The TEM image clearly showed that the Pd NPs were highly dispersed in the channels of the mesoporous shells, having an average particle size of about 5 nm (Fig. 8B). In contrast, the Pt NPs supported on the bare ZSM-5 crystals aggregated easily to form larger particles with a less uniformity (Fig. 8A). The mesopores, possessing a confining effect, would be benefit to enhance the distribution of precise metal particles.

3.2 Catalytic properties of Pt/MZ_x@MSA in the hydrocracking of n-hexadecane

The catalytic activity of the core-shell structured composites after supporting Pt NPs was evaluated in the hydrocracking of *n*-hexadecane as a probe molecule. *n*-hexadecane was a good model for a saturated paraffin jet fuel, and use of a pure compound avoids many of the difficulties of interpretation of results that occurs when dealing with complex results. The products for hydrocracking of n-hexadecane could be divided into three groups according to the carbon numbers: $C_1 – C_4$, C_5 - C_{11} and C_{12} - C_{15}. C_5 - C_{11} were very important products, which were main components of high-value middle distillates. The bifunctional catalytic properties of $Pt/MZ_{AT0.2\text{-}PI0.02}$@MSA were compared with conventional Pt/ZSM-5 and $Pt/MZ_{AT0.2\text{-}PI0.02}$ catalysts. Pt/ZSM-5 showed 74.2 % conversion of *n*-hexadecane and 50.5 % selectivity for C_5 - C_{11} (Table 2, No. 1). $Pt/MZ_{AT0.2\text{-}PI0.02}$ showed slightly increased conversion (76.0 %) and C_5 - C_{11} selectivity (53.8 %) (Table 2, No. 2). The

improvement is presumed to the contribution of the mesopores created by NaOH treatment. Irregularly distributed inside ZSM-5 crystals, these mesopores would shorten the diffusion paths of *n*-hexadecane molecules and help them to reach the zeolite acid sites more easily. Besides, the middle distillates of C_5 - C_{11} could diffuse out of the micropores rapidly, which inhibited a deep cracking to suppress the formation gaseous hydrocarbons of C_1 - C_4. Pt/MSA with a Si/Al molar ratio of 61 showed only 12.6 % conversion of *n*-hexadecane owing to its relatively weak acidity and small amount of acid sites (Table 2, No. 6). On the other hand, Pt/$MZ_{AT0.2\text{-}PI0.02}$@MSA, with a core-shell structure of about 76 wt.% of mesoporous ZSM-5 and 24 wt.% Al-containing mesoporous shell, showed the highest *n*-hexadecane conversion of 80.4 % and a C_5 - C_{11} selectivity of 58.0 % (Table 2, No. 3). The mechanical mixture of Pt/$MZ_{AT0.2\text{-}PI0.02}$ and Pt/MSA was also employed to the hydrocracking. It gave a lower conversion of *n*-hexadecane (75.9 %) and a lower selectivity for C_5 - C_{11} (55.4 %) (Table 2, No. 7). The two types of catalytic active sites (Pt NPs and acid sites) existed in the physical mixture but separately in a distance of microscale, which further reflected the importance of the direct connected and highly opened junction between $MZ_{AT0.2\text{-}PI0.02}$ core and Al-containing mesoporous shell. The core-shell structured composite materials of Pt/$MZ_{AT0.1}$@MSA and Pt/$MZ_{AT0.2}$@MSA, prepared in the absence of piperidine during NaOH disilication, both showed a lower *n*-hexadecane conversion and a lower C_5 - C_{11} selectivity Pt/$MZ_{AT0.2\text{-}PI0.02}$ (Table 2, Nos. 3 - 5). Thus, the appropriate shell thickness and mesopores incorporated into ZSM-5 cores were also very important for this reaction.

For more detailed comparison, Pt/$MZ_{AT0.2\text{-}PI0.02}$@MSA always showed a higher conversion of *n*-hexadecane and a higher selectivity for C_5 - C_{11} than Pt/ZSM-5 during 80 h time-on-stream (Fig. 9), and under different WHSV (Fig. S5 and S6) as well as at different temperatures (Fig. S7 and S8).

Scheme 1 summarizes graphically the synthesis of the core-shell composite comprising a mesoporous ZSM-5 core and Al-containing mesoporous shell by combining together desilication and assembly. Coating mesoporous ZSM-5 with Al-containing mesoporous shell and further incorporating Pt NPs into the formed mesopores , the composite material of Pt/$MZ_{AT0.2\text{-}PI0.02}$@MSA demonstrated the most active hydrocracking property and the highest selectivity for middle distillates. The micropores and two sets of mesopores may construct a hierarchical pore system in a synergistic way. The existence of mesopores either in shell or in core could reduce more effectively the diffusion path length of bulky molecules. The mesoporous shell with a large surface area could effectively capture the bulky *n*-hexadecane molecules like a pump,[54] which then gave a higher conversion than Pt/ZSM-5 and Pt/$MZ_{AT0.2\text{-}PI0.02}$. Besides, the mesoporous shell coated on the mesoporous ZSM-5 could reduce the contact of product molecules on the solid acid sites of zeolites, which inhibited the deep cracking of middle distillates of C_5 - C_{11} to gaseous hydrocarbons of C_1 - C_4. Through the synthetic strategy planned in this research, we could define the existence of aluminosilicate species in the shells of $MZ_{AT0.2\text{-}PI0.02}$@MSA. Thus, the *n*-hexadecane molecules underwent pre-cracking on the acid sites available in the shells, which improved the selectivity of middle distillates. Then the middle distillates could

enter into the cores containing strong acid sites where a further reaction occurred to improve the total conversion. As shown above, the novel shells of $MZ_{AT0.2\text{-}PI0.02}$@MSA possessed a "concrete with crushed stone"-like mesostructure, and then a greatly improved hydrothermal stability. It would be a more promising catalyst in real applications than those composite materials with pure mesosilica as shell.

4 Conclusions

We have successfully prepared a hierarchical core-shell structured composite materials comprising mesoporous zeolite core and Al-containing mesoporous shell by controlled desilication and P123 copolymer-assisted self-assembly in the absence of external silica and alumina sources. This material provides suitable scaffolds for supporting Pt NPs. With a tunable shell thickness, the core-shell structured materials possesse three sets of pores from exterior mesoporous shell to inner micro/mesoporous core, which effectively reduces the diffusion path length. The mesoporous shells contain the MFI aluminosilicate species and exhibit a good hydrothermal stability. Confining the Pt NPs into the mesoporous shells leads to a novel catalyst with bifunctional abilities for hydrocracking reactions, which exhibits an enhanced hydrocracking activity for of *n*-hexadecane and an increased selectivity for C_5 - C_{11}. The results are of referential importance to the design and synthesis of other multifunctional core-shell materials.

Acknowledgements

We gratefully acknowledge the National Natural Science Foundation of China (21373089, U1162102), PhD Programs Foundation of Ministry of Education (2012007613000), the National Key Technology R&D Program (2012BAE05B02), and the Shanghai Leading Academic Discipline Project (B409).

References

1 N. Choudary and D. N. Saraf, *Ind. Eng. Chem. Prod. Res. Dev*., 1975, **14**, 74-83.

2 Y. Miki, S. Yamadaya, M. Oba and Y Sugimoto, *J. Catal*., 1983, **83**, 371-383.

3 R. A. Corbett, *Oil Gas J*., 1989, **26**, 42-46.

4 D. J. O'Rear, *Ind. Eng. Chem. Res*., 1987, **26**, 2337-2344.

5 N. Y. Chen, *Oil & Gas J*., 1968, **66**, 151-154.

6 M. S. Rana, V. Samano, J. Ancheyta and J. A. I. Diaz, *Fuel*, 2007, **86**, 1216-1231.

7 Y. S. Tao, H. Kanoh and L. Abrams, K. Kaneko, *Chem. Rev*., 2006, **106**, 896-910.

8 J. C. Groen, J. C. Jansen, J. A. Moulijin and J. Pérez-Ramírez, *J. Phys. Chem. B*., 2004, **108**, 13062-13065.

9 J. C. Groen, T. Bach, U. Ziese, A. M. Paulaime, K. P. De Jong, J. A. Moulijin and J. Pérez-Ramírez, *J. Am. Chem. Soc*., 2005, **127**, 10792-10793.

10 R. M. Dessau, E. W. Valyocsik and N. H. Goeke, *Zeolites*, 1992, **12**, 776-779.

11 M. Ogura, S. Shinomiya, J. Tateno, Y. Nara, E. Kikuchi and M. Matsukata, *Chem. Lett*., 2000, 882-883.

12 M. Ogura, S. Shinomiya, J. Tateno, Y. Nara, M. Nomura, E. Kikuchi and M.

Matsukata, *Appl. Catal., A*, 2001, **219**, 33-43.

13 T. Suzuki and T. Okuhara, *Microporous Mesoporous Mater*., 2001, **43**, 83-89.

14 J. C. Groen, J. Pérez-Ramírez and L.A.A. Peffer, *Chem.Lett*., 2002, **31**, 94-95.

15 J. C. Groen, L. A. A. Peffer, J. A. Moulijn and J. Pérez-Ramírez, *Colloids Surf. A*., 2004, **241**, 53-58.

16 J. C. Groen, L. A. A. Peffer, J. A. Moulijn and J. Pérez-Ramírez, *Microporous Mesoporous Mater*., 2004, **69**, 29-34.

17 L. Su, L. Liu, J. Zhuang, H. Wang, Y. Li, W. Shen, Y. Xu and X. Bao, *Catal. Lett*., 2003, **91**, 155-167.

18 S. van Donk , A. H. Janssen , J. H. Bitter and K. P. de Jong , *Catal. Rev*., 2003, **45** , 297-319.

19 C. J. H. Jacobsen, C. Madsen, J. Houzvicka, I. Schmidt and A. Carlsson, *J. Am. Chem. Soc*., 2000, **122**, 7116-7117.

20 C. Madsen and C. J. H. Jacobsen, *Chem. Commun*., 1999, **8**, 673-674.

21 A. H. Janssen, I. Schmidt, C. J. H. Jacobsen, A. J. Koster and K. P. De Jong, *Microporous Mesoporous Mater*., 2003, **65**, 59-75.

22 J. Wang, J. C. Groen, W. Yue, W. Zhou and M. Coppens, *J. Mater. Chem*., 2008, **18**, 468-474.

23 Y. Tao, H. Kanoh and K. Kaneko, *J. Am. Chem. Soc*., 2003, **125**, 6044-6045.

24 H. Wang and T. J. Pinnavaia, *Angew. Chem., Int. Ed*., 2006, **45**, 7603-7606.

25 F. S. Xiao, L. F. Wang, C. Y. Yin, K. F. Lin, Y. Di, J. X. Li, R. R. Xu, D. S. Su, R. Schlögl, T. Yokoi and T. Tatsumi, *Angew. Chem., Int. Ed*., 2006, **45**, 3090-3093.

26 R. Srivastava, M. Choi and R. Ryoo, *Chem. Commun*., 2006, **43**, 4489-4491.

27 D. P. Serrano, J. Aguado, J. M. Escola, J. M. Rodríguez and A. Peral, *Chem. Mater*., 2006, **18**, 2462-2464.

28 M. Choi, H. S. Cho, R. Srivastava, C. Venkatesan, D. H. Choi and R. Ryoo, *Nat. Mater*., 2006, **5**, 718-723.

29 A. Corma, M.-J. Díaz-Cabañas, J. Martínez-Triguero and F. Rey, J. Rius, *Nature*, 2002, **418**, 514-517.

30 A. H. Janssen, A. J. Koster and K. P. de Jong, *Angew. Chem. Int. Ed*., 2001, **40**, 1102-1104.

31 J. C. Groen, J. A. Moulijn and J. Pérez-Ramírez, *J. Mater. Chem*., 2006, **16**, 2121-2131.

32 J. C. Groen, S. Abello, L. A. Villaescusa and J. Pérez-Ramírez, *Microporous Mesoporous Mater*., 2008, **114**, 93-102.

33 A. Bonilla, D. Baudouin and J. Pérez-Ramírez, *J. Catal*., 2009, **265**, 170-180.

34 Ł. Mokrzycki, B. Sulikowski and Z. Olejniczak, *Catal. Lett*., 2009, **127**, 296-303.

35 J. C. Groen, T. Sano, J. A. Moulijn and J. Pérez-Ramírez, *J. Catal*., 2007, **251**, 21-27.

36 J. Pérez-Ramírez, S. Abello, L. A. Villaescusa and A. Bonilla, *Angew. Chem*., 2008, **120**, 8031-8035; *Angew. Chem. Int. Ed*., 2008, **47**, 7913-7917.

37 L. Xu, Y. Ren, H. Wu, Y. Liu, Z. Wang, Y. Zhang, J. Xu, H. Peng and P. Wu, *J. Mater. Chem*., 2011, **21**, 10852-10858.

38 X. Qian, J. Du, B. Li, M. Si, Y. Yang, Y. Hu, G. Niu, Y. Zhang, H. Xu, B. Tu, Y.

Tang and D. Zhao, *Chem. Sci*., 2011, **2**, 2006-2016.

39 X. W. Lou, L. A. Archer and Z. Yang, *Adv. Mater*., 2008, **20**, 3987-4019.

40 D. Chen, L. L. Li, F. Q. Tang and S. Qi, *Adv. Mater*., 2009, **21**, 3804-3807.

41 Y. Bouizi, I. Diaz, L. Rouleau and V. P. Valtchev, *Adv. Funct. Mater*., 2005, **15**, 1955-1960.

42 M. V. Barmatova, I. D. Ivanchikova, E. I. El'Kina, A. N. Shmakov, M. S. Mel'Gunov and V. B. Fenelonov, *Appl. Surf. Sci*., 2010, **256**, 5513-5519.

43 W. Schartl, *Nanoscale*, 2010, **2**, 829-843.

44 J. Kim, H. S. Kim, N. Lee, T. Kim, H. Kim, T. Yu, I. C. Song, W. K. Moon and T. Hyeon, *Angew. Chem. Int. Ed*., 2008, **47**, 8438-8441

45 Y. Lu, Y. Yin, Z. Li and Y. Xia, *Nano Lett*., 2002, **2**, 785-788.

46 Y. Deng, D. Qi, C. Deng, X. Zhang and D. Zhao, *J. Am. Chem. Soc*., 2008, **130**, 28-29.

47 J. Ge, Q. Zhang, T. Zhang and Y. Yin, *Angew. Chem. Int. Ed*., 2008, **47**, 8924-8928.

48 J. S. Yu, S. B. Yoon, Y. J. Lee and K. B. Yoon, *J. Phys. Chem. B*., 2005, **109**, 7040-7045.

49 Y. Han, P. Pitukmanorom, L. Zhao and J. Y. Ying, *Small*, 2011, **7**, 326-332.

50 H. G. Peng, L. Xu, H. H. Wu, K. Zhang and P. Wu, *Chem. Commun*., 2013, **49**, 2709-2711.

51 H. G. Peng, L. Xu, H. H. Wu, Z. D. Wang, Y. M. Liu, X. H. Li, M. Y. He and P. Wu, *Microporous Mesoporous Mater*., 2012, **153**, 8-17.

52 F. Coloma, A. Sepúlveda-Escribano, J.L.G. Fierro and F. Rodriguez-Reinoso, *Appl. Catal., A: Gen*., 1997, **53**, 165-183.

53 W. Zhang, T. R. Pauly and T. J. Pinnavaia, *Chem. Mater*., 1997, **9**, 2491-2498.

54 X. F. Qian, B. Li, Y. Y. Hu, G. X. Niu, D. Y. H. Zhang, R. C. Che, Y. Tang, D. S. Su, A. M. Asiri and D. Y. Zhao, *Chem. Eur. J*., 2012, **18**, 931-939.

55 D. Lesthaeghe, P. Vansteenkiste, T. Verstraelen, A. Ghysels, C. E. A. Kirschhock, J. A. Martens, V. Van Speybroeck and M. Waroquier, *J. Phys. Chem. C*., 2008, **112**, 9186-9191.

56 Y. Li, W. H. Zhang, L. Zhang, Q. H. Yang, Z. B. Wei, Z. C. Feng and C. Li, *J. Phys. Chem. B*., 2004, **108**, 9739-9744.

Figure captions

Fig. 1 Typical XRD patterns of ZSM-5 (a), $MZ_{AT0.2\text{-}PI0.02}$ (b), $MZ_{AT0.1}$@MSA (c), $MZ_{AT0.2\text{-}PI0.02}$@MSA (d) and $MZ_{AT0.2}$@MSA (e).

Fig. 2 SEM and TEM images of ZSM-5 (Si/Al=38) (a, b), $MZ_{AT0.2\text{-}PI0.02}$ (c, d), $MZ_{AT0.1}$@MSA (e, f), $MZ_{AT0.2\text{-}PI0.02}$@MSA (g, h) and $MZ_{AT0.2}$@MSA (i, j).

Fig. 3 HRTEM images of $MZ_{AT0.2\text{-}PI0.02}$@MSA for the cross-section between mesoporous shell and meso-ZSM-5 core (A), and for the area with coexisted hierarchical pores (B), that is, mesopores formed by P123-assisted self-assembly on zeolite crystal surface (a), original 10-MR micropores of MFI structure (b), and irregular intracrystal mesopores created by desilication (c).

Fig. 4 N_2 adsorption-desorption isotherms (A) and pore size distribution (B) of ZSM-5 (a), $MZ_{AT0.2\text{-}PI0.02}$ (b) and $MZ_{AT0.2\text{-}PI\ 0.02}$@MSA (c).

Fig. 5 SEM images of pristine $MZ_{AT0.2\text{-}PI0.02}$@MSA (a), pristine $MZ_{AT0.2\text{-}PI0.02}$@MSA-TEOS (b), $MZ_{AT0.2\text{-}PI0.02}$@MSA after hydrothermal treatment at 403 K (c), $MZ_{AT0.2\text{-}PI0.02}$@MSA-TEOS after hydrothermal treatment at 403 K (d), $MZ_{AT0.2\text{-}PI0.02}$@MSA after steaming treatment at 1023 K(e), $MZ_{AT0.2\text{-}PI0.02}$@MSA-TEOS after steaming at 1023 K (f).

Fig. 6 NH_3-TPD profiles of ZSM-5 (Si/Al=38) (a), $MZ_{AT0.2\text{-}PI0.02}$ $MZ_{AT0.2\text{-}PI0.02}$@MSA (c), a mechanical mixture of $MZ_{AT0.2\text{-}PI0.02}$ (76 wt %) and MSA (24 wt %) (d), and pure mesoporous sample of MSA (e).

Fig. 7 Pyridine-adsorbed IR spectra of ZSM-5 (Si/Al=38) (a), $MZ_{AT0.2\text{-}PI0.02}$ (b), $MZ_{AT0.2\text{-}PI0.02}$@MSA (c), a mechanical mixture of $MZ_{AT0.2\text{-}PI0.02}$ (76 wt %) and MSA

(24 wt %) of $MZ_{AT0.2\text{-}PI0.02}$&MSA (d), and pure MSA (e). The pyridine desorption was carried out by evacuation at 423 K for 1 h.

Fig. 8 HRTEM images of Pt/ZSM-5 (A) and Pt/$MZ_{AT0.2\text{-}PI0.02}$@MSA (B). The inset shows the size distribution of Pt particles.

Fig. 9 The hydrocracking of *n*-hexadecane over Pt/ZSM-5 (a) and Pt/$MZ_{AT0.2\text{-}PI0.02}$@MSA (b), the conversion of *n*-hexadecane *vs.* time on stream (A) and the selectivity of C_5 - C_{11} *vs.* conversion (B). Reaction conditions: catalyst, 0.1 g; feed of *n*-hexadecane, 1.0 mL h^{-1}; flow rate of H_2, 45 mL min^{-1}; WHSV, 7.7 h^{-1}; H_2/C_{16} molar ratio, 35; temperature, 653 K; atmospheric pressure.

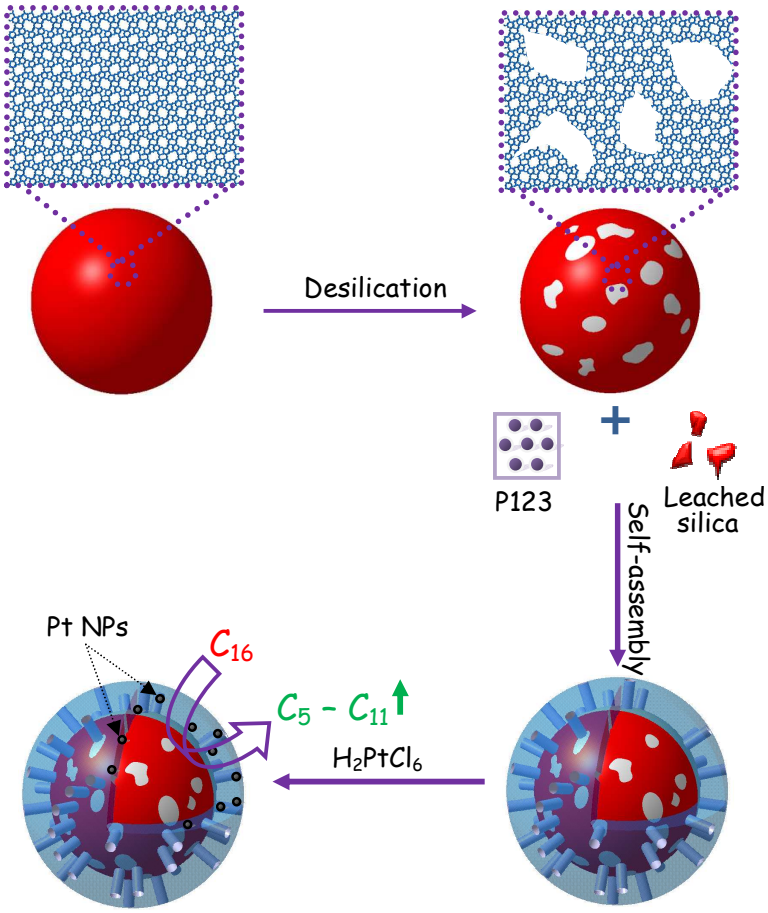

Scheme 1 Schematic of the synthesis of the core-shell composite comprising a mesoporous ZSM-5 core and Al-containing mesoporous silica shell by separated processes of desilication and self-assembly.

Table 1 Textural properties of pristine ZSM-5 and the core-shell structured composite molecular sieves MZ_x@MSA with different shell thickness [a]

No.	Samples	Shell thickness [b] (nm)	S_{BET} ($m^2 g^{-1}$)	S_{ext} ($m^2 g^{-1}$)	V_{tot} [c] ($cm^3 g^{-1}$)	V_{micro} [d] ($cm^3 g^{-1}$)	V_{meso} ($cm^3 g^{-1}$)	Yield [e] (%)
1	ZSM-5	-	316	12	0.21	0.16	-	100
2	$MZ_{AT0.2\text{-}PI0.02}$	-	452	220	0.72	0.13	0.59	69
3	$MZ_{AT0.1}$@MSA	60	450	243	0.42	0.11	0.31	81 (93)
4	$MZ_{AT0.2\text{-}PI0.02}$@MSA	150	539	358	0.61	0.09	0.52	69 (91)
5	$MZ_{AT0.2}$@MSA	300	451	291	0.51	0.08	0.43	43 (90)

[a] Given by N_2 adsorption at 77 K. [b] Given by TEM images. [c] Calculated at P/P_0=0.99. [d] Calculated from *t*-plot. [e] The percentage of obtained solid product relative the amount of ZSM-5 used. The values in parentheses indicate the yield after secondary self-assembly with P123 copolymer.

Table 2 Catalytic hydrocracking of *n*-hexadecane over Pt/$MZ_{AT0.2\text{-}PI0.02}$@MSA and related materials[a].

No.	Catalyst	*n*-$C_{16}H_{34}$ conv. (%)	Selectivity (%)		
			$C_{1\text{-}4}$	$C_{5\text{-}11}$	$C_{12\text{-}15}$
1	Pt/ZSM-5	74.2	48.7	50.5	0.8
2	Pt/$MZ_{AT0.2\text{-}PI0.02}$	76.0	45.6	53.8	0.6
3	Pt/$MZ_{AT0.2\text{-}PI0.02}$@MSA	80.4	41.4	58.0	0.6
4	Pt/$MZ_{AT0.1}$@MSA	76.8	44.3	54.2	0.5
5	Pt/$MZ_{AT0.2}$@MSA	72.3	37.9	55.2	1.2
6	Pt/MSA	12.6	31.2	67.4	1.8
7	Pt/$MZ_{AT0.2\text{-}PI0.02}$&MSA	75.9	43.8	55.4	0.8

[a] Reaction conditions: cat., 0.1 g; feed of *n*-hexadecane, 1.0 mL h^{-1}; WHSV, 7.7 h^{-1}; flow rate of H_2, 45 mL min^{-1}; temperature, 573 K; atmospheric pressure.

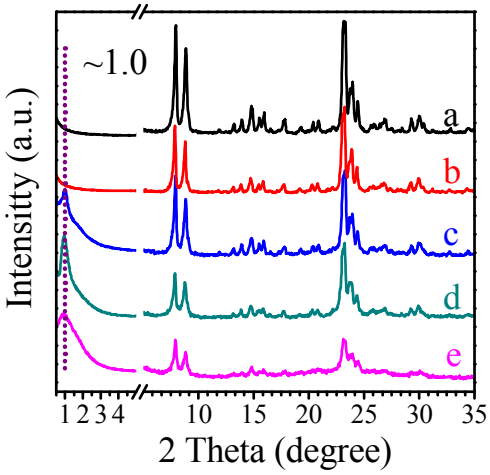

Fig. 1 Typical XRD patterns of ZSM-5 (a), $MZ_{AT0.2\text{-}PI0.02}$ (b), $MZ_{AT0.1}$@MSA (c), $MZ_{AT0.2\text{-}PI0.02}$@MSA (d) and $MZ_{AT0.2}$@MSA (e).

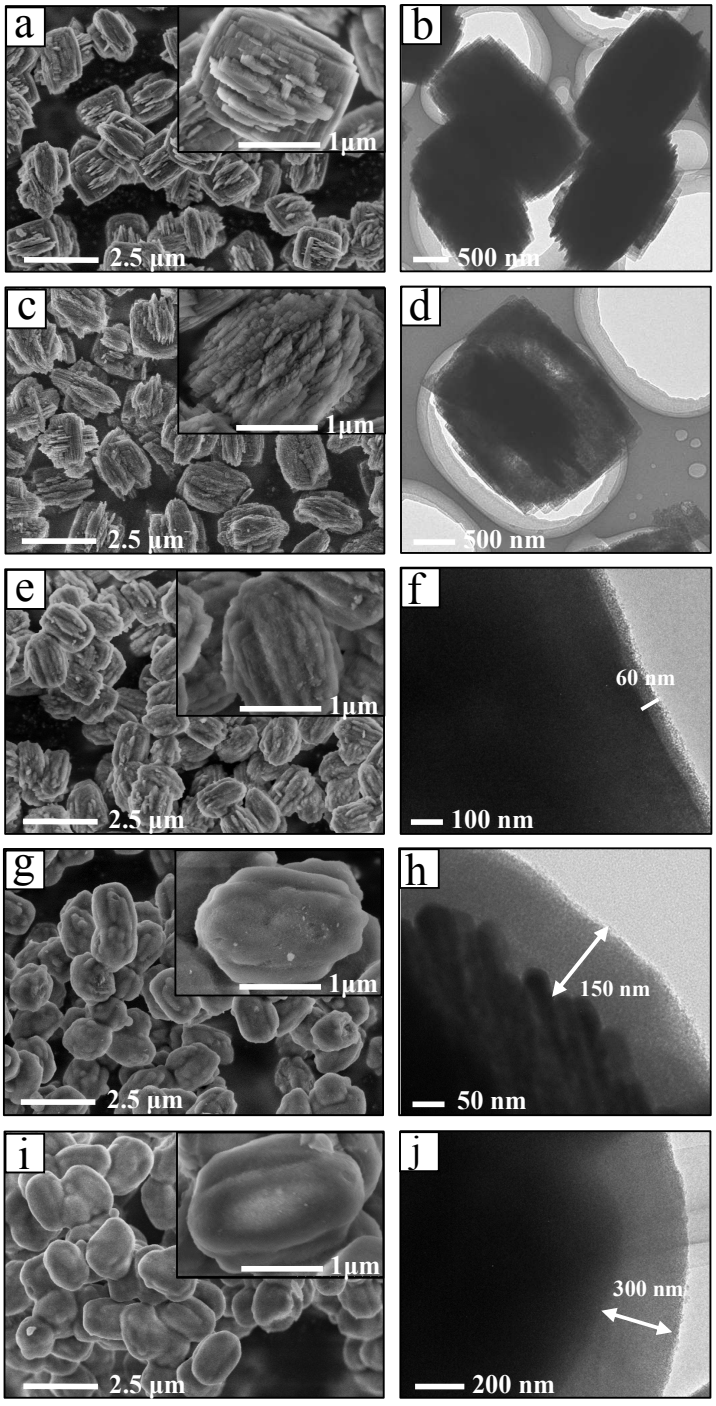

Fig. 2 SEM and TEM images of ZSM-5 (Si/Al=38) (a, b), $MZ_{AT0.2\text{-}PI0.02}$ (c, d), $MZ_{AT0.1}$@MSA (e, f), $MZ_{AT0.2\text{-}PI0.02}$@MSA (g, h) and $MZ_{AT0.2}$@MSA (i, j).

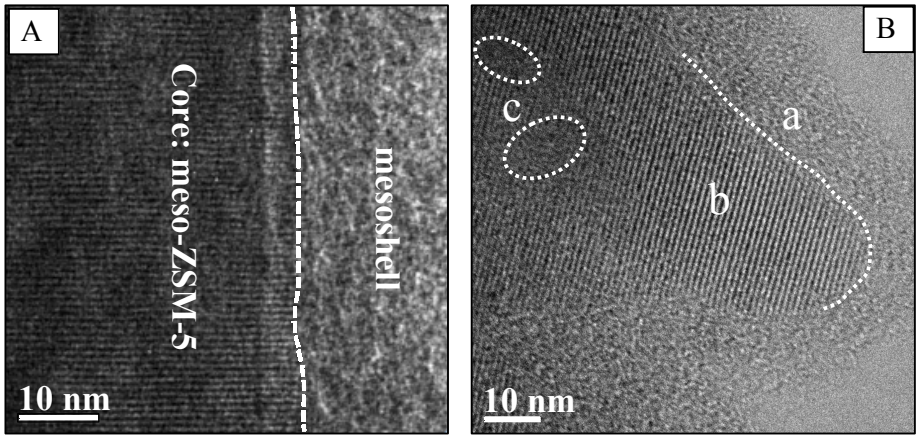

Fig. 3 HRTEM images of $MZ_{AT0.2\text{-}PI0.02}$@MSA for the cross-section between mesoporous shell and meso-ZSM-5 core (A), and for the area with coexisted hierarchical pores (B), that is, mesopores formed by P123-assisted self-assembly on zeolite crystal surface (a), original 10-MR micropores of MFI structure (b), and irregular intracrystal mesopores created by desilication (c).

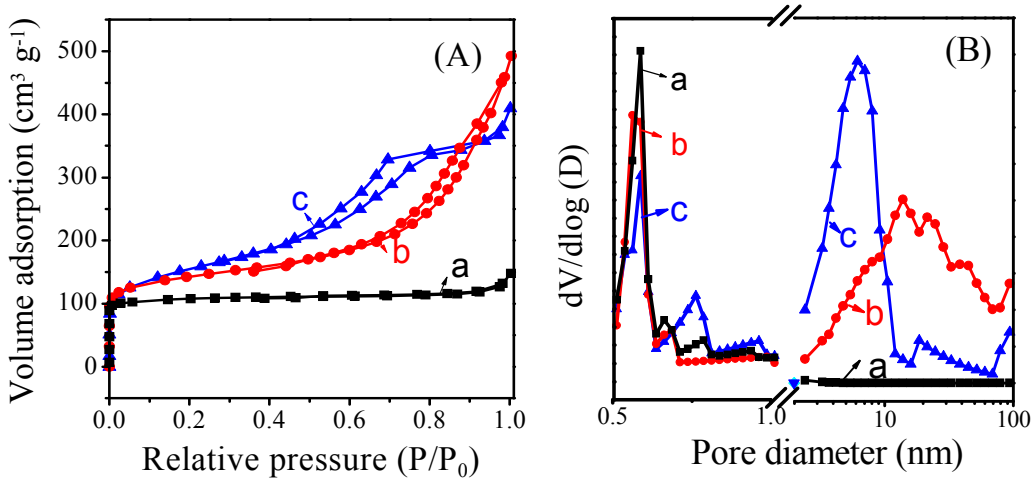

Fig. 4 N_2 adsorption-desorption isotherms (A) and pore size distribution (B) of ZSM-5 (a), $MZ_{AT0.2\text{-}PI0.02}$ (b) and $MZ_{AT0.2\text{-}PI\ 0.02}$@MSA (c).

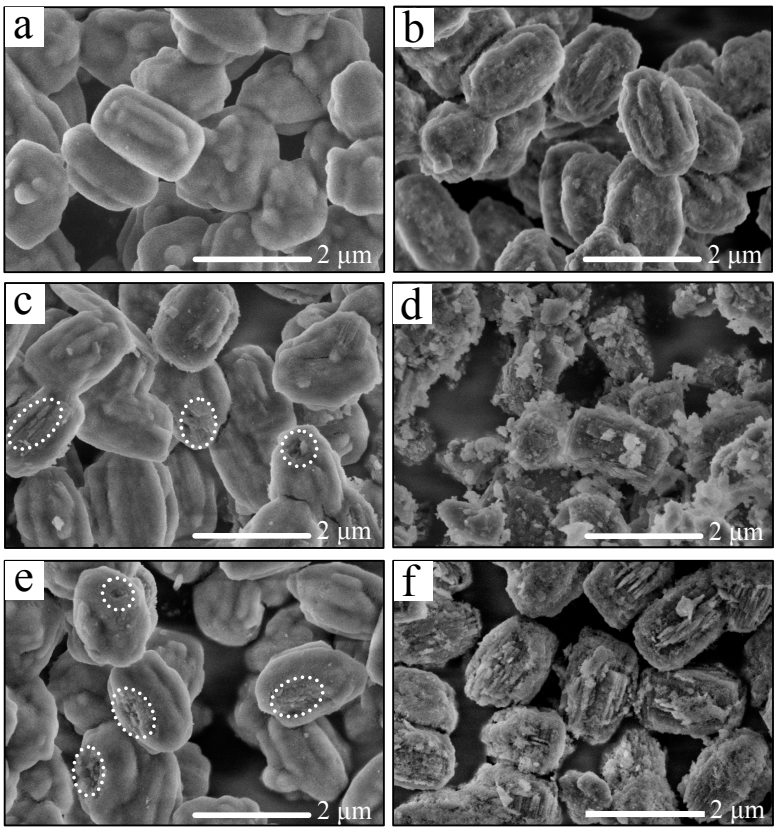

Fig. 5 SEM images of pristine $MZ_{AT0.2\text{-}PI0.02}$@MSA (a), pristine $MZ_{AT0.2\text{-}PI0.02}$@MSA-TEOS (b), $MZ_{AT0.2\text{-}PI0.02}$@MSA after hydrothermal treatment at 403 K (c), $MZ_{AT0.2\text{-}PI0.02}$@MSA-TEOS after hydrothermal treatment at 403 K (d), $MZ_{AT0.2\text{-}PI0.02}$@MSA after steaming treatment at 1023 K(e), $MZ_{AT0.2\text{-}PI0.02}$@MSA-TEOS after steaming at 1023 K (f).

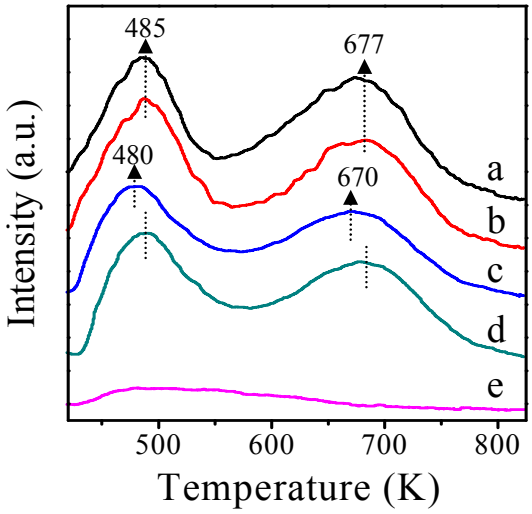

Fig. 6 NH_3-TPD profiles of ZSM-5 (Si/Al=38) (a), $MZ_{AT0.2\text{-}PI0.02}$ $MZ_{AT0.2\text{-}PI0.02}$@MSA (c), a mechanical mixture of $MZ_{AT0.2\text{-}PI0.02}$ (76 wt %) and MSA (24 wt %) (d), and pure mesoporous sample of MSA (e).

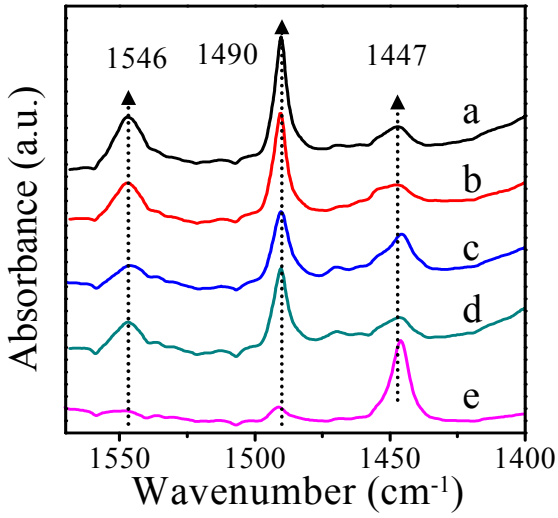

Fig. 7 Pyridine-adsorbed IR spectra of ZSM-5 (Si/Al=38) (a), $MZ_{AT0.2\text{-}PI0.02}$ (b), $MZ_{AT0.2\text{-}PI0.02}$@MSA (c), a mechanical mixture of $MZ_{AT0.2\text{-}PI0.02}$ (76 wt %) and MSA (24 wt %) of $MZ_{AT0.2\text{-}PI0.02}$&MSA (d), and pure MSA (e). The pyridine desorption was carried out by evacuation at 423 K for 1 h.

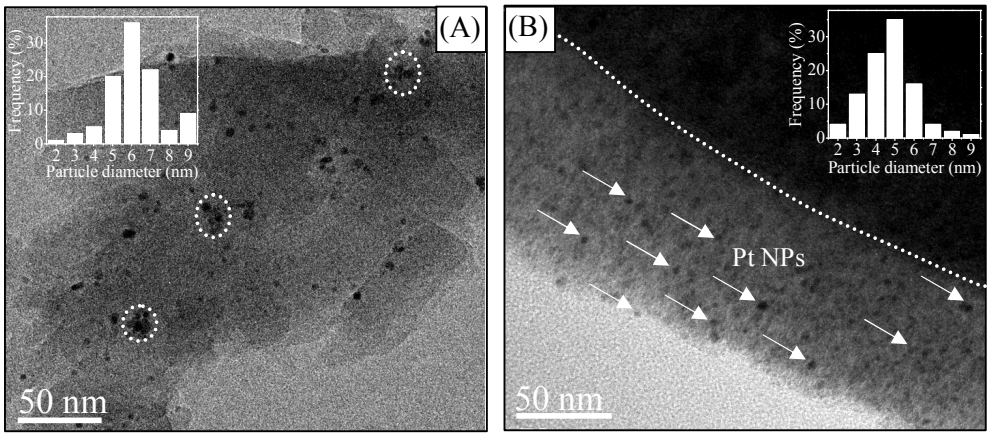

Fig. 8 HRTEM images of Pt/ZSM-5 (A) and Pt/$MZ_{AT0.2\text{-}PI0.02}$@MSA (B). The inset shows the size distribution of Pt particles.

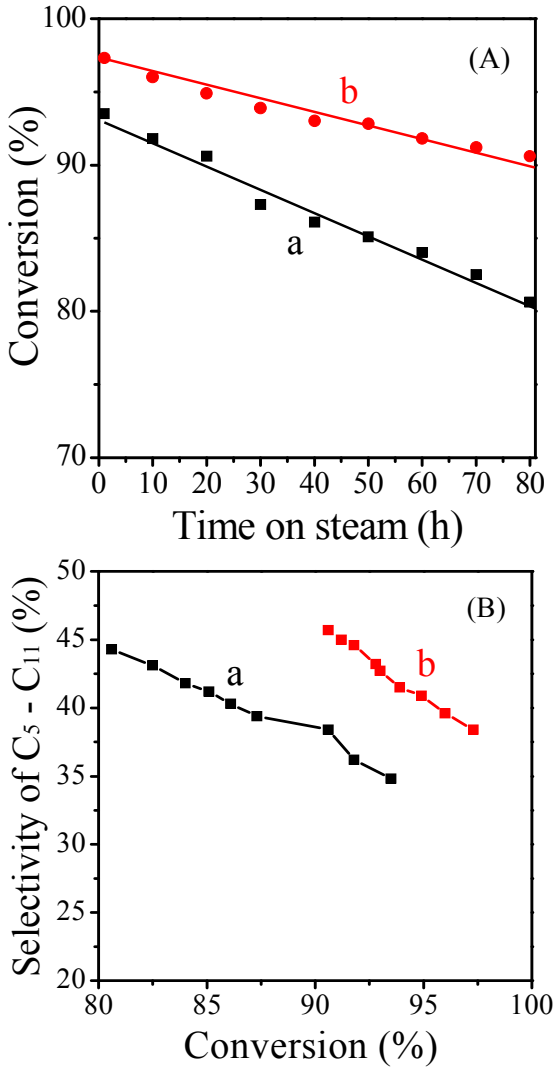

Fig. 9 The hydrocracking of *n*-hexadecane over Pt/ZSM-5 (a) and Pt/$MZ_{AT0.2\text{-}PI0.02}$@MSA (b), the conversion of *n*-hexadecane *vs.* time on stream (A) and the selectivity of C_5 - C_{11} *vs.* conversion (B). Reaction conditions: catalyst, 0.1 g; feed of *n*-hexadecane, 1.0 mL h^{-1}; flow rate of H_2, 45 mL min^{-1}; WHSV, 7.7 h^{-1}; H_2/C_{16} molar ratio, 35; temperature, 653 K; atmospheric pressure.